catalysts

MDPI

Article

The 'Green' Ni-UGSO Catalyst for Hydrogen Production under Various Reforming Regimes

Mostafa Chamoumi and Nicolas Abatzoglou *

Department of Chemical Engineering and Biotechnological Engineering, Université de Sherbrooke, 2500, Boulevard de l'Université, Sherbrooke, QC J1K 2R1, Canada; Mostafa.Chamoumi@usherbrooke.ca
* Correspondence: Nicolas.Abatzoglou@usherbrooke.ca; Tel.: +1-819-821-7904

Abstract: A new spinelized Ni catalyst (Ni-UGSO) using $Ni(NO_3)_2 \cdot 6H_2O$ as the Ni precursor was prepared according to a less material intensive protocol. The support of this catalyst is a negative-value mining residue, UpGraded Slag Oxide (UGSO), produced from a TiO_2 slag production unit. Applied to dry reforming of methane (DRM) at atmospheric pressure, T = 810 °C, space velocity of 3400 mL/(h·g) and molar CO_2/CH_4 = 1.2, Ni-UGSO gives a stable over 168 h time-on-stream methane conversion of 92%. In this DRM reaction optimization study: (1) the best performance is obtained with the 10–13 wt% Ni load; (2) the Ni-UGSO catalysts obtained from two different batches of UGSO demonstrated equivalent performances despite their slight differences in composition; (3) the sulfur-poisoning resistance study shows that at up to 5.5 ppm no Ni-UGSO deactivation is observed. In steam reforming of methane (SRM), Ni-UGSO was tested at 900 °C and a molar ratio of H_2O/CH_4 = 1.7. In this experimental range, CH_4 conversion rapidly reached 98% and remained stable over 168 h time-on-stream (TOS). The same stability is observed for H_2 and CO yields, at around 92% and 91%, respectively, while H_2/CO was close to 3. In mixed (dry and steam) methane reforming using a ratio of H_2O/CH_4 = 0.15 and CO_2/CH_4 = 0.97 for 74 h and three reaction temperature levels (828 °C, 847 °C and 896 °C), CH_4 conversion remains stable; 80% at 828 °C (26 h), 85% at 847 °C (24 h) and 95% at 896 °C (24 h). All gaseous streams have been analyzed by gas chromatography. Both fresh and used catalysts are analyzed by scanning electron microscopy-electron dispersive X-ray spectroscopy (SEM-EDXS), X-ray diffraction (XRD), and thermogravimetric analysis (TGA) coupled with mass spectroscopy (MS) and BET Specific surface. In the reducing environment of reforming, such catalytic activity is mainly attributed to (a) alloys such as FeNi, $FeNi_3$ and Fe_3Ni_2 (reduction of $NiFe_2O_4$, $FeNiAlO_4$) and (b) to the solid solution NiO-MgO. The latter is characterized by a molecular distribution of the catalytically active Ni phase while offering an environment that prevents C deposition due to its alkalinity.

Keywords: green nickel catalyst; Ni-UGSO; mining residue; spinel; basic support; solid solution; NiO–MgO; hydrogen; syngas; dry; steam and mixed reforming

Citation: Chamoumi, M.; Abatzoglou, N. The 'Green' Ni-UGSO Catalyst for Hydrogen Production under Various Reforming Regimes. *Catalysts* **2021**, *11*, 771. https://doi.org/10.3390/catal11070771

Academic Editors: Woohyun Kim and Kyubock Lee

Received: 17 May 2021
Accepted: 23 June 2021
Published: 25 June 2021

1. Introduction

Several research works on nickel-based reforming catalysts are devoted to the development of their supports. The catalyst presented in this work valorizes a mining residue by using it as a support, allowing the production of renewable hydrogen from green catalysts and responding to the different spheres of sustainable development.

Worldwide, H_2 is produced mainly from hydrocarbons using steam reforming of methane (SRM) (Reaction (R1)). Partial oxidation (POX) (Reaction (R2)) or dry reforming (DRM) (Reaction (R3)) are good candidates too. However, their use in the industry is limited due to certain drawbacks, namely, the relatively fast catalyst deactivation [1].

$$CH_4 + H_2O \leftrightarrow CO + 3H_2 \qquad (\Delta H^\circ_{298} = 206\ MJ/kmol) \qquad (R1)$$

$$CH_4 + 1/2O_2 \leftrightarrow CO + 2H_2 \qquad (\Delta H^\circ_{298} = -38\ MJ/kmol) \qquad (R2)$$

$$CH_4 + CO_2 \leftrightarrow 2CO + 2H_2 \qquad (\Delta H^\circ_{298} = 247\ MJ/kmol) \qquad (R3)$$

SRM is the largest scale process for the production of H_2 by natural gas conversion. CH_4 is converted with steam on supported Ni catalysts in a highly endothermic reaction. The SRM reaction is conducted in heated tubular reactors to achieve the high temperatures needed, making steam reforming a major energy consumer.

Secondary reactions of carbon deposition also occur such as:

$$2CO \leftrightarrow C + CO_2 \qquad \text{Boudouard} \qquad (R4)$$

$$CH_4 \leftrightarrow C + 2H_2 \qquad CH_4 \text{ dissociation} \qquad (R5)$$

$$H_2 + CO \leftrightarrow C + H_2O \qquad H_2O \text{ production} \qquad (R6)$$

$$2H_2 + CO_2 \leftrightarrow C + 2H_2O \qquad H_2O \text{ production} \qquad (R7)$$

An excess of water makes it possible to drive Reaction (R6) towards the formation of synthesis gas and minimize carbon formation. In fact, by reacting CO with H_2O according to the water-gas-shift (WGS) Reaction (R8), the CO becomes CO_2, thus producing more hydrogen and increasing the H_2/CO ratio:

$$CO + H_2O \leftrightarrow CO_2 + H_2 \qquad (\Delta H^\circ_{298} = -41\ MJ/kmol) \qquad (R8)$$

Because the SRM reaction is endothermic, it requires high-temperature conditions (T > 800 °C) to increase conversion and decrease carbon formation while increasing H_2 and CO yields. Relatively high working pressures (20–40 bar) are also used industrially [2,3]. This process, despite its importance, has the major disadvantage of being energy-intensive, a situation which is made worse by the use of excess water.

In the catalytic POX (Reaction (R2)), CH_4 is converted with oxygen or air to form H_2 and CO with a ratio of $H_2/CO = 2$. This ratio of 2 is ideal for most downstream processes, making partial oxidation of methane a simple, one-step process. Unlike SRM, the POX of methane is slightly exothermic.

In the last decades, the constant development of DRM (Reaction (R3)) is mainly due to:

(a) the use 2 GHGs (CH_4 and CO_2); the technology is under study and making its first steps at industrial demonstration scale [4];

(b) the production of a valuable syngas (CO + H_2) with a molar $H_2/CO = 1$, which is essential, among other things, for the production of methanol and wax according to Fischer–Tropsch [5,6]. More recently, Topsoe developed a technology, called ReShift™ that uses a significant amount of CO_2 for making synthesis gas (syngas; H_2 + CO) without the traditional challenge of carbon formation [7].

DRM, being an endothermic reaction, requires high temperatures (higher than 650 °C). Otherwise, the side reactions below may take place [8].

$$CO_2 + H_2 \leftrightarrow CO + H_2O \qquad \text{Reverse WGS} \qquad (R9)$$

$$2CO \leftrightarrow C + CO_2 \qquad \text{Boudouard} \qquad (R4)$$

$$CH_4 \leftrightarrow C + 2H_2 \qquad CH_4 \text{ dissociation} \qquad (R5)$$

$$C + H_2O \leftrightarrow CO + H_2 \qquad \text{C gasification} \qquad (R10)$$

The production of hydrogen H_2 by reforming reactions mainly uses Ni-based catalysts under conditions that prevent their deactivation by the formation of carbon (C) [9–12]. Carbon formation results mainly from the Boudouard reaction (Reaction (R4)) and the decomposition of CH_4 (Reaction (R5)) [10,13].

One way to overcome the drawback of coking is the strong interaction between the active metal (Ni) and the support that prevents the formation of carbon and the sintering of Ni [14].

For catalysts supported by alumina (Al_2O_3), the spinel phase formed ($NiAl_2O_4$) allows high conversion of CH_4 with low formation of C during SRM reactions [15]. Likewise, the nickel-alumina spinel catalyst supported on alumina and yttria-stabilized zirconia ($NiAl_2O_4$-/Al_2O_3-YSZ), developed by our research group, has demonstrated significant resistance to poisoning when compared to standard Ni/Al_2O_3-YSZ formulations in the case of diesel steam reforming [16–18].

The addition of promoters in the formulation of the catalyst has also been the subject of several research studies [19–21]. Luna et al. [22] studied the effect of K, Ca, Sn and Mn on a Ni/Al_2O_3 catalyst. The authors indicated that the presence of K improved the stability significantly with a slight decrease in activity after 30 h of TOS. Siahvashi et al. [23] studied the DR of propane and showed that the addition of K to the Ni–Mo catalyst supported by Al_2O_3 increased the CO yield with a significant decrease in carbon deposition.

In addition, several studies have shown the beneficial effect of the basicity of supports. Thus, the addition of MgO to a Ni/Al_2O_3 catalyst improved the stability of the catalyst at high temperatures by forming $MgAl_2O_4$ spinel. The strong adsorption of CO_2 on the basic surface of MgO is considered the main mechanism of carbon formation prevention [24]. The work carried out by Ranjbar et al. [25], on the addition of Ca, shows an increase in the activity of the catalyst and its resistance to carbon deposition.

Rio Tinto Iron and Titanium (RTIT), a wholly-owned subsidiary of Rio Tinto, has been operating for several years at the Tio mine, the largest ilmenite deposit ($FeTiO_3$) in the world, located 43 km northeast of Havre-Saint-Pierre, Quebec. A world leader in the industry, RTIT has developed and implemented a proprietary process called UpGraded Slag (UGS) on the site of the Sorel-Tracy metallurgical complex (Quebec). UGS produces titanium slag with the highest TiO_2 content (94.5%) on the market from the Ilmenite of the North Shore. However, this process generates a large amount of UGS oxide residue (noted UGSO), sent directly to the tailings deposit to end up in the landfill. Concerned by the accumulation of large quantities of this residue and the importance of its footprint, RTIT has for several years made significant efforts to find other solutions. Avoiding depositing these UGSOs in landfill tailings ponds by upgrading them has become a major and urgent challenge.

This waste, whose chemical composition has been presented in our previous paper [26] has been considered an excellent nickel-based catalyst support candidate. Indeed, UGSO already contains oxides recognized for their ability to avoid carbon formation, the main cause of these catalysts' deactivation.

In our previous papers [26–28], we have developed a simple and easy solid-state method of preparing a new generation of Ni-UGSO catalyst using UGSO as a support and Ni as the active metal.

The first results obtained, when applying the Ni-UGSO to DRM, show good catalytic performances with no carbon deposit [26].

The objective of this work consists of, on the one hand, an optimization of the DRM, and on the other hand, the study of the catalytic activity of this new Ni-UGSO catalyst in other types of CH_4 reforming, namely SRM, mixed (dry and steam) methane reforming and its sulfur-poisoning resistance. In this work, Ni-UGSO BT designates the fresh catalyst before treatment reforming (BT) and Ni-UGSO AT designates the catalyst after treatment reforming.

2. Results

2.1. Characterization of Fresh Catalysts Ni-UGSO BT

As presented in our previous article [26], by ICP-MS analysis, the Ni-UGSO BT catalyst shows a Ni content of 13.9 ± 1.6 wt%; BET analysis gave a specific surface area of 3.94 ± 0.26 m^2/g and SEM analyses have shown that the catalyst particles have a lamellar morphology and average size of 168 ± 59 nm.

Compared to oxide residue before testing (UGSO-BT), XRD patterns [26] of the new catalyst sample before catalytic testing (Ni-UGSO-BT) showed, in addition to the spinel

peaks present in UGSO-BT, the appearance of new peaks corresponding to Ni-based spinels ($NiFe_2O_4$ and $FeNiAlO_4$). XRD patterns also showed three other components at the same 2θ = 37.31, 43.30, 63.40, 75.5 and 79.1° [26]. These peaks corresponded to the remaining MgO, NiO, and solid solution NiO-MgO. These results agree with those of Requies et al. [29], who study the partial oxidation of methane; the diffraction patterns of Ni/MgO catalysts containing 20 and 30 wt% showed the formation of a solid solution between NiO and MgO at 2θ of 37.2, 43.1, 62.6, 75.0 and 78.9°.

2.2. Thermodynamics of DRM and SMR Reactions

CH_4 and CO_2 conversions (DRM), CH_4 and H_2O conversion (SRM), and the thermodynamic equilibrium composition of the products, under a pressure of 1 atm, were calculated using the FactSage 7.3 software (FactSage 7.3; Thermfact/CRCT, Montreal, QC, Canada; www.crct.polymtl.ca and GTT-Technologies, Aachen, Germany, www.gtt-technologies.de; 2019). Full data from the thermodynamic study are provided in Part A of the Supplementary Materials.

The study showed that, at thermodynamic equilibrium, starting at 850 °C, the DRM reaction showed a molar ratio of $H_2/CO = 1$ and conversion rates of 97% for CH_4 and 95% for CO_2. However, it was only at or above 950 °C that the formation of carbon was fully inhibited.

The SRM reaction showed, at or above 850 °C, a molar ratio of $H_2/CO = 3$ and CH_4 and H_2O conversion rates of 94% and 95%, respectively. At or above this temperature (850 °C), carbon formation no longer occurred.

Taking all presented data into consideration, it would be more reasonable to study the catalytic performance of the Ni-UGSO catalyst in the temperature range of 800–900 °C, where conversion was practically complete and carbon formation was still marginally thermodynamically possible.

2.3. Ni-UGSO Performance as a Catalyst for DRM

2.3.1. Experimental Evaluation of Catalyst Activity and Stability

In the DRM of our previous work [26], a molar CO_2/CH_4 was heated at 810 °C in the presence of 0.3 g of catalyst. A comparison of the catalytic activity of Ni-UGSO (Q_{CO2} = 7.08 mL/min, Q_{CH4} = 7.26 mL/min and GHSV = 2867 mL/(h·g)) with UGSO (Q_{CO2} = 7.63 mL/min, Q_{CH4} = 7.35 mL/min and GHSV = 2996 mL/(h·g)) showed that a maximum CH_4 conversion of 30% was obtained after 30 min of reaction in the presence of UGSO, which gradually decreased and reached 18% after 4 h of reaction. Under the same experimental conditions in the presence of the new Ni-UGSO catalyst, the conversion of CH_4 quickly reached 87% and remains stable during the 4 h of reaction.

Activity and stability of the new Ni-UGSO catalyst were assessed for 7 days of DRM in the same conditions as above at a molar ratio of $CO_2/CH_4 = 1.2$ (Q_{CO2} = 9.30 mL/min and Q_{CH4} = 7.76 mL/min and GHSV = 3412 mL/(h·g)) [26]. CH_4 conversion rapidly reached 92% and remains stable over 168 h TOS. The same stability was observed for H_2 and CO yields, which were at around 82% and 87%, respectively, with a molar H_2/CO ratio close to 1, which was closer to the thermodynamic equilibrium. An activity loss of approximately 5% over seven days TOS was observed.

The various techniques for characterizing spent catalysts (XRD, SEM-EDX, XPS, TGA-MS) showed no carbon deposition.

2.3.2. Influence of the Active Phase Content on the Catalytic Activity

This study aimed to optimize the content of the active phase (Ni) necessary to carry out the DRM while obtaining a suitable conversion. Five nickel mass contents were chosen: 3%, 6%, 9%, 10% and 13%. Catalysts were calcined at 900 °C for 12 h. The DRM reaction was carried out at 840 °C with a CO_2/CH_4 ratio of 1.25 (Q_{CO2} = 9.62 mL/min and Q_{CH4} = 7.71 mL/min) without Ar and a GHSV of 3500 mL/(h·gcat).

Figure 1 shows the evolution of CH_4 conversion along the reforming tests. Part B of the supplementary information presents figures of CO_2 conversions (Figure S6, Supplementary Materials), H_2 yield (Figure S7, Supplementary Materials) and the H_2/CO ratio (Figure S8, Supplementary Materials).

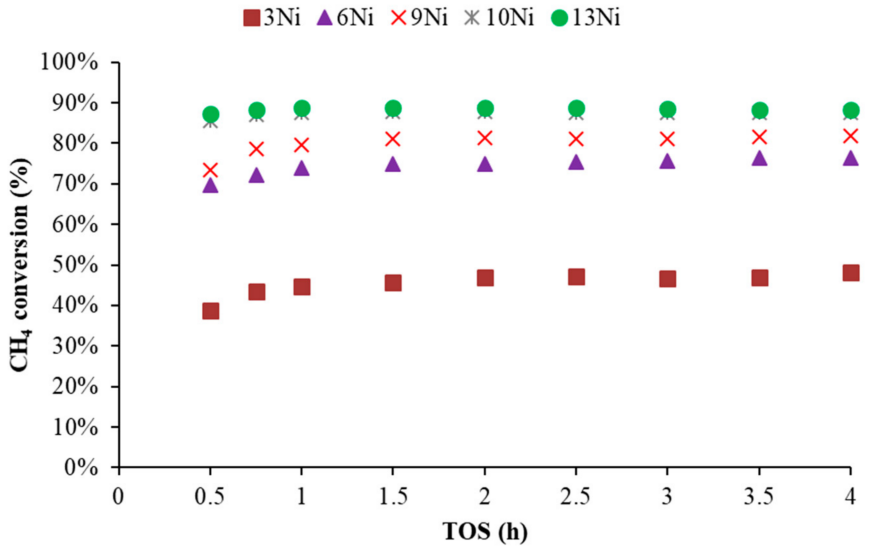

Figure 1. Effect of Ni content: evolution of CH_4 conversion as a function of time (CO_2/CH_4 = 1.25, 842 °C, Catalysts are calcined at 900 °C for 12 h).

At 3% Ni, the catalyst had the lowest catalytic activity compared to the others because the CH_4 and CO_2 conversions did not exceed 50% and 60%. The same applied to the H_2 yield, which was in the order of 65%. The best performance was obtained with the 10% Ni catalyst; it was equivalent to the performance of the 13% Ni catalyst. The data obtained from H_2/CO (0.5) and X-CO_2/X-CH_4 (1.3) conversion rates indicated the significant role of the reverse-water-gas-shift (RWGS) reaction. However, these two ratios tended towards thermodynamic values (H_2/CO = 1, X-CO_2/X-CH_4 = 1) as the Ni content increased.

These results corroborated those obtained from the XRD analyses (Figure 2), where the intensity of the peaks attributed to different species of Ni oxides (spinel $NiFe_2O_4$, $FeNiAlO_4$ and solid solution NiO-MgO (red arrow) was a function of the Ni content.

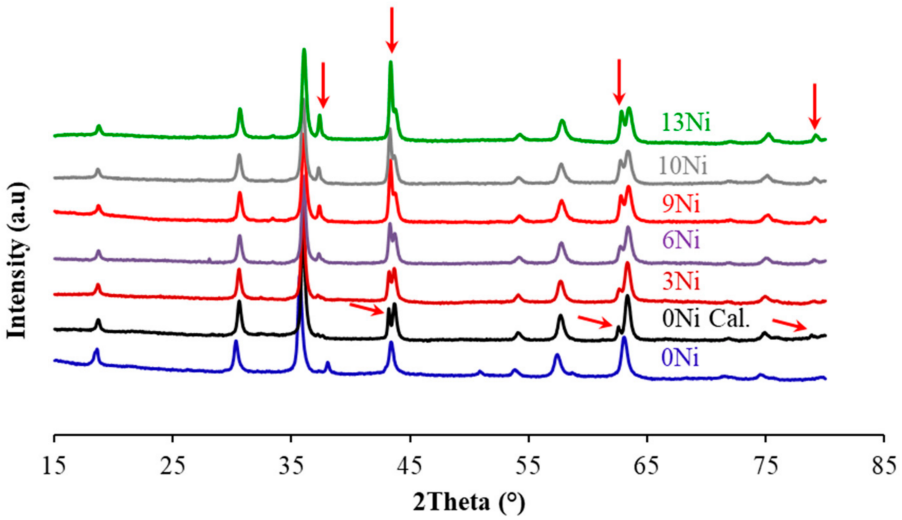

Figure 2. XRD of catalysts as a function of Ni content.

Average catalyst surface BET as a function of Ni-loading (Table 1) shows that the BET decreased slightly as a function of Ni-loading. This could be due to some agglomeration of the particles. The same was also observed on the UGSO support (without Ni), whose surface area decreased from 38 m^2/g to 6 m^2/g after calcination at 900 °C for 12 h.

Table 1. Average catalyst surface BET as function of Ni-loading.

Ni (wt%)	3	6	9	10	13
S_{BET} (m^2/g)	5.4 ± 0.5	5.0 ± 0.2	4.5 ± 0.2	4.4 ± 0.4	3.8 ± 0.4

Figure 3 below shows SEM photos of the Ni-UGSO catalyst as a function of Ni-loading. These figures show that, whatever the Ni content, the particles kept their lamellar shape.

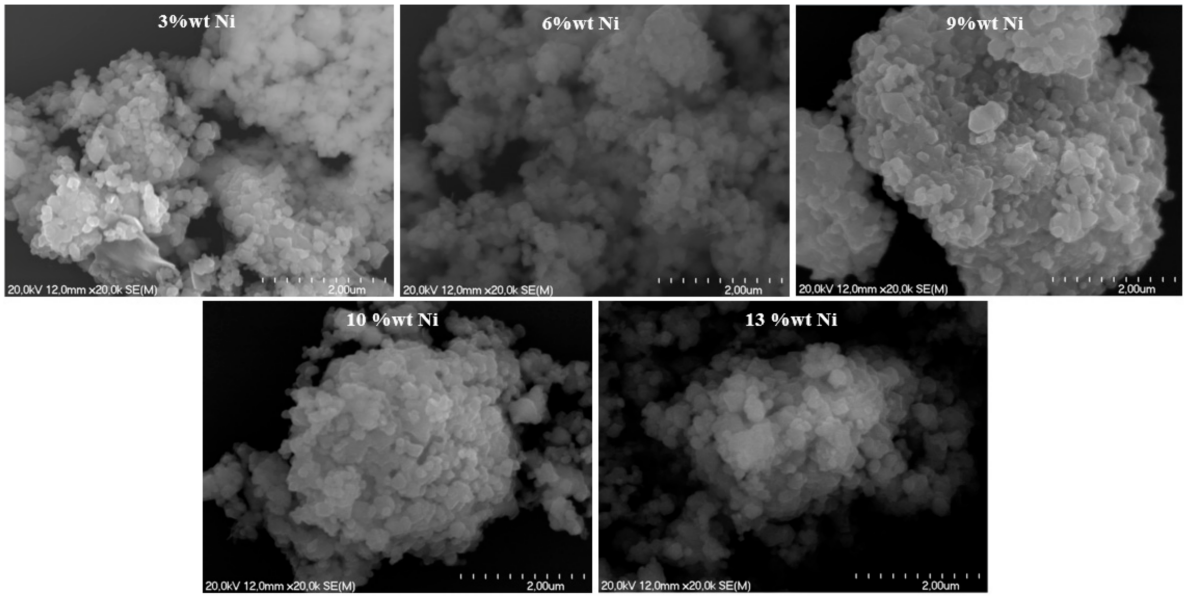

Figure 3. SEM photos of the Ni-UGSO catalyst as a function of Ni-loading.

The mapping study shows, in all cases, a good dispersion of the Ni (Figure S9, Supplementary Materials).

2.3.3. Influence of Catalyst Calcination Time

Three catalysts were obtained by calcination at 900 °C for 1 h, 3 h and 12 h. The catalytic performances of these three solids was studied with 0.3 g of Ni-UGSO catalyst at 840 °C using a CO_2/CH_4 molar ratio = 1.2 (Q_{CO2} = 9.75 mL/min and Q_{CH4} = 8.20 mL/min) without Ar. The results obtained, presented in Figure 4, showed that the performances of the catalyst calcined for 3 h at 900 °C was similar to that of the catalyst treated for 12 h at the same temperature. Moreover, the catalyst with 1 h of heat treatment at 900 °C gave the best performance. Consequently, 1 h of calcination would be sufficient to obtain a catalyst giving CH_4 conversions exceeding 95%.

Examination of the XRDs of these catalysts (Figure S10, Supplementary Materials) indicated that the longer the calcination time, the more the peaks at 2θ = 43° and 63° (two of the four representative peaks of the catalyst) became sharper. These indications and those of the specific surfaces presented in Table 2 went in the same direction, thus confirming the effect of prolonged exposure of the catalyst to the heat treatment on particle size. The best performances obtained by the catalyst calcined for 1 h was, therefore, related to its higher specific surface area compared to the other two. This is an important result because it is related to the energy consumption during the eventual commercial manufacturing of the catalyst.

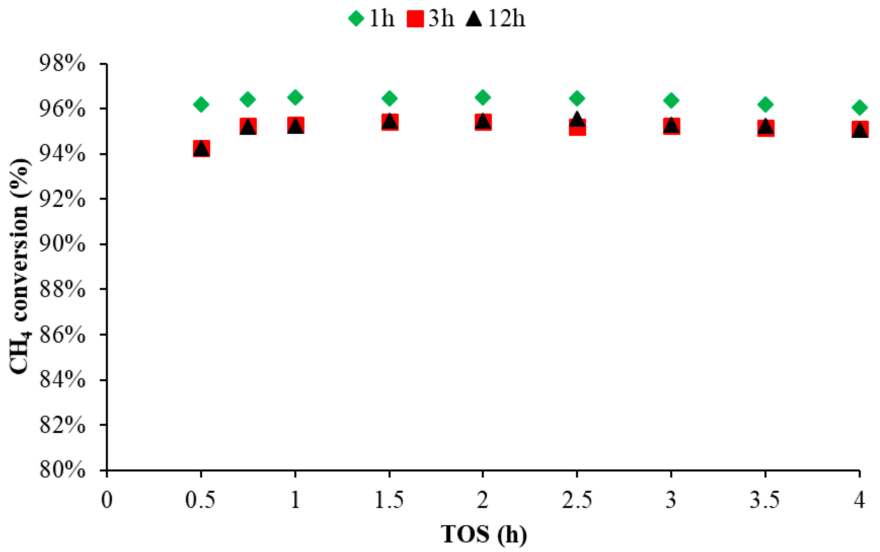

Figure 4. Effect of calcination time of Ni-UGSO catalyst with 13% Ni (wt%): evolution of CH_4 conversion as a function of time (CO_2/CH_4 = 1.2, 840 °C).

Table 2. Average catalyst surface BET as function of calcination time of Ni-UGSO catalyst with 13% Ni (wt%).

Cal. Time (h)	1	3	12
S_{BET} (m^2/g)	5.0 ± 0.2	4.7 ± 0.2	3.8 ± 0.4

2.3.4. Representativeness of UGSO Mining Residue Lots

A second batch (L2) of UGSO was compared with the first (L1) to evaluate the impact of a variation of the UGSO composition on the Ni-UGSO catalyst performance.

As shown in Table 3, the ICP-MS analysis shows that the constitutive elements of the residue remain unchanged despite the variation in their contents. The balance is oxygen.

Table 3. ICP-MS analysis of two batches of UGSO (wt%).

	Fe	Mg	Al_3	Ca	Mn	V_5	Ti_2	Cr	Zn
UGSO-L1	31.11	17.98	5.23	1.28	1.68	1.46	0.49	0.47	0.01
UGSO-L2	34.04	21.09	6.84	1.58	1.82	1.71	0.52	0.56	0.01
Variation	9.44%	17.32%	30.70%	24.13%	8.24%	16.74%	5.38%	18.50%	0.00%

XRD patterns (Figure S11, Supplementary Materials) showed that, although the structures of UGSO-L1 and UGSO-L2 seemed different, UGSO-L2 was identical to that of the first batch calcined at 900 °C/12 h (UGSO-L1_Cal.). This suggests that the second batch may have undergone additional calcination before its disposal in the RTIT Landfill [30]. It should be noted that only the L1 batch was slightly different in terms of phases. All other batches received subsequently had the same phases, and their calcination did not bring any change to the material, as shown by the calcination carried out on L3 (Figure S12, Supplementary Materials). Otherwise, despite the slight difference in composition, the catalytic activity of the different batches used in the reforming tests showed similar catalytic activities.

The corresponding Ni-UGSO-L1 and Ni-UGSO-L2 catalysts, both at 13% Ni (wt%), were prepared according to the same protocol of improved solid-state reaction and calcined at 900 °C for 1 h.

The XRDs of the two catalysts (Figure S13, Supplementary Materials) showed that both catalysts obtained by adding Ni as active metal had the same structure (a slight difference was observed for the peak at 2θ = 63.45°).

The reforming reactions were carried out at 840 °C on 0.3 g of Ni-UGSO-L1 or L2 calcined for 1 h using a CO_2/CH_4 molar ratio = 1.2 (Q_{CO2} = 9.45 mL/min and Q_{CH4} = 7.68 mL/min) without Ar and a GHSV = 3400 mL/(h·gcat). The results obtained (Figure 5) showed that the two catalysts had the same CH_4 conversions. Despite a slight difference of the composition, the Ni-UGSO catalysts obtained from these two batches of tested residues demonstrated equivalent performance during DRM.

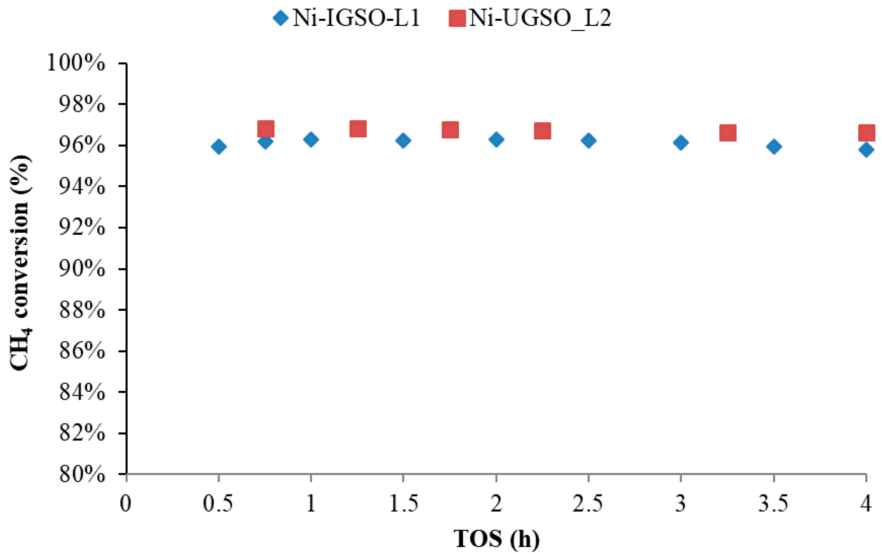

Figure 5. CH4 conversion over TOS at 840 °C, CO_2/CH_4 = 1.2.

Comparison of Ni-UGSO-L1 (batch 1) and Ni-UGSO-L2 (batch 2) calcined at 900 °C for 1 h.

2.3.5. Ni-UGSO Sulfur Poisoning Resistance

Ni-UGSO sulfur poisoning resistance was assessed for 5 h of DRM with a molar ratio of CO_2/CH_4 = 0.96 at 810 °C under 1.5 ppm, 5.5 ppm and 12 ppm of H_2S.

Up to 5.5 ppm, the catalyst showed no deactivation. A slight deactivation (3%) was observed at 12 ppm and remained stable throughout the 1 h exposure of the catalyst to H_2S at the reported concentrations (Figure 6).

As shown in the XRD of used catalysts (Figure S14, Supplementary Materials), the amount of S was so low that the peaks corresponding to Ni-S were not detected. However, a more in-depth study of the resistance of Ni-UGSO to sulfides was carried out, by our group research, at higher concentrations (275 ppm of H_2S) on dry autothermal ethane reforming [31]. XRD, BET, SEM and TGA analysis are used. XRD showed the formation of new phases such as NiFe, NiS and FeS. In TGA analysis, weight losses observed were attributed to the endothermal decomposition of $NiSO_4$, which might be formed by oxidation of the NixSy species; this decomposition was described by the following equation: $NiSO_4(s) = NiO(s) + SO_2(g) + \frac{1}{2} O_2(g)$.

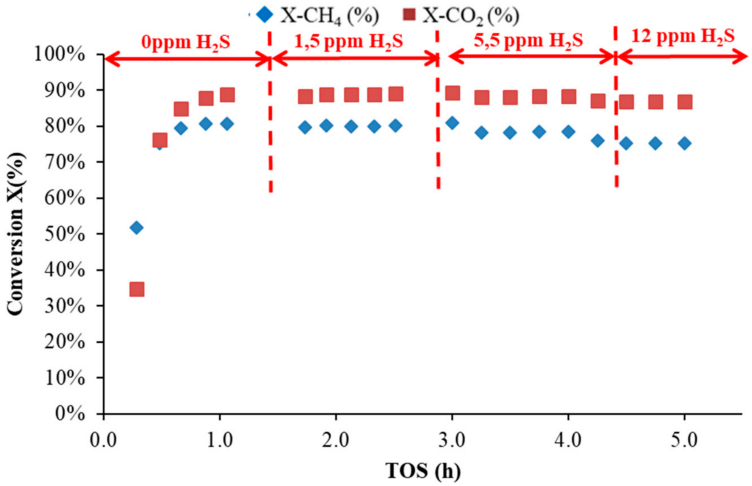

Figure 6. Catalytic performances of Ni-UGSO on DRM at low H_2S loads (CO_2/CH_4 = 0.96, 810 °C).

2.4. Ni-UGSO Performance as a Catalyst for SRM

SRM on Ni-based catalysts is currently the only industrially used method for hydrogen production [32]. S/C ratios more than 3 [32] are used at the expense of energy to avoid catalyst deactivation by carbon deposition. The excess of steam is beneficial in gasifying a portion of the carbonaceous deposits on the catalyst surface and, therefore, improving the carbon gasification [32,33]. Nevertheless, the higher amounts of H_2O also lead to an enrichment of the product in H_2 due to the enhancing the WGS reaction.

Ni-UGSO stability in SRM was evaluated for seven days at 900 °C with a molar ratio of H_2O/CH_4 = 1.7 (Q_{H2O} = 13.94 mL/min, Q_{CH4} = 8.20 mL/min and Q_{Ar} = 17.15 mL/min), well below industrial ratios.

The results obtained showed that, during the 7 days of reaction, CH_4 conversion remained stable at around 98%, with a molar H_2/CO ratio in the products close to 3. This is a clear indication that, at these experimental conditions, the reaction reached thermodynamic equilibrium (Figure 7).

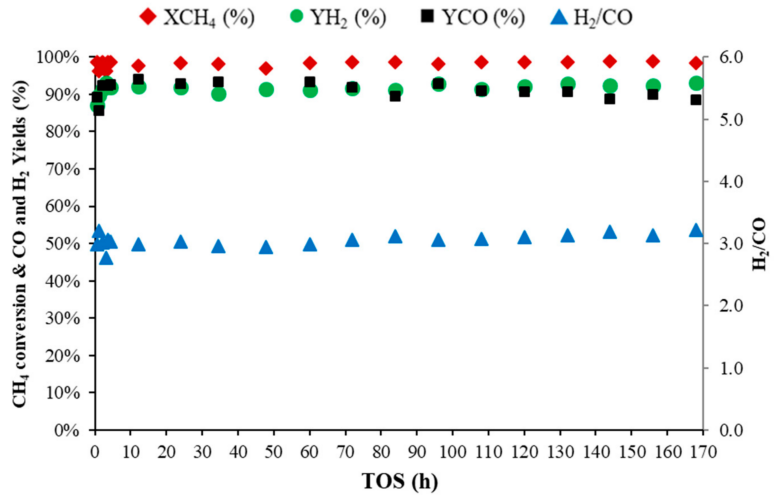

Figure 7. Catalytic performances of Ni-UGSO on SRM (H_2O/CH_4 = 1.7, 900 °C).

It is important to note that no trace of carbon was detected on the spent catalyst, as shown by the XRD analysis (Figure S15, Supplementary Materials) and SEM-EDX analyses (Figure 8). It should also be noted that the small peak of carbon observed in the EDX of the spent catalyst (Ni-UGSO AT) was identical to that of the fresh catalyst (Ni-UGSO-BT). As mentioned in our previous work [26], this carbon peak is attributed to the $CaCO_3$

carbonates, the remaining carbon traces used during the UGS process reduction step. It can also be attributed to atmospheric CO_2 absorbed or adsorbed. However, the SEM photos (Figure 8) showed the appearance of spherical particles in the spent catalyst compared to the fresh catalyst.

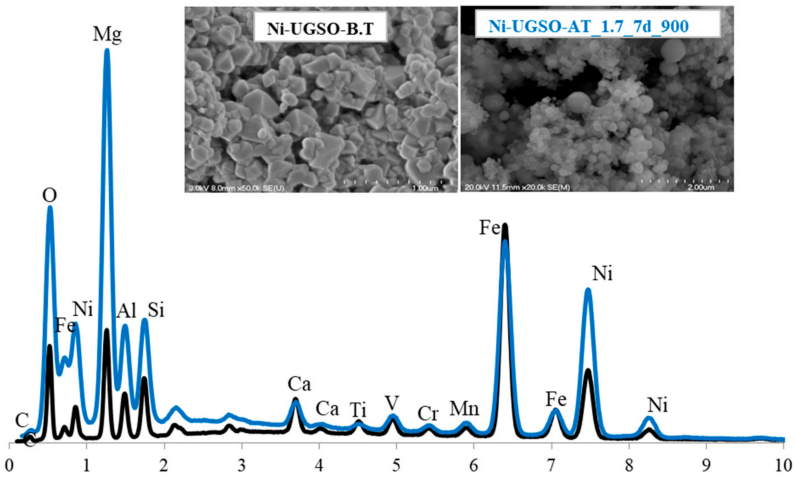

Figure 8. SEM and EDX of Ni-UGSO BT and Ni-UGSO AT (7 days, H_2O/CH_4 = 1.7, 900 °C).

The mapping analysis of the fresh catalyst (Figure 9) and used catalyst (Figure 10) showed that the former has a homogeneous morphology as well as a good dispersion of the active metal (Ni) as well as those of the support (Mg, Al and Fe). After 7 days of reaction, the spent catalyst (Figure 10) showed the appearance of certain spherical particles consisting mainly of Ni and Fe. As described in the interpretation proposed during the DRM, these spherical particles were attributed to Ni–Fe alloys formed by reduction during the DRM.

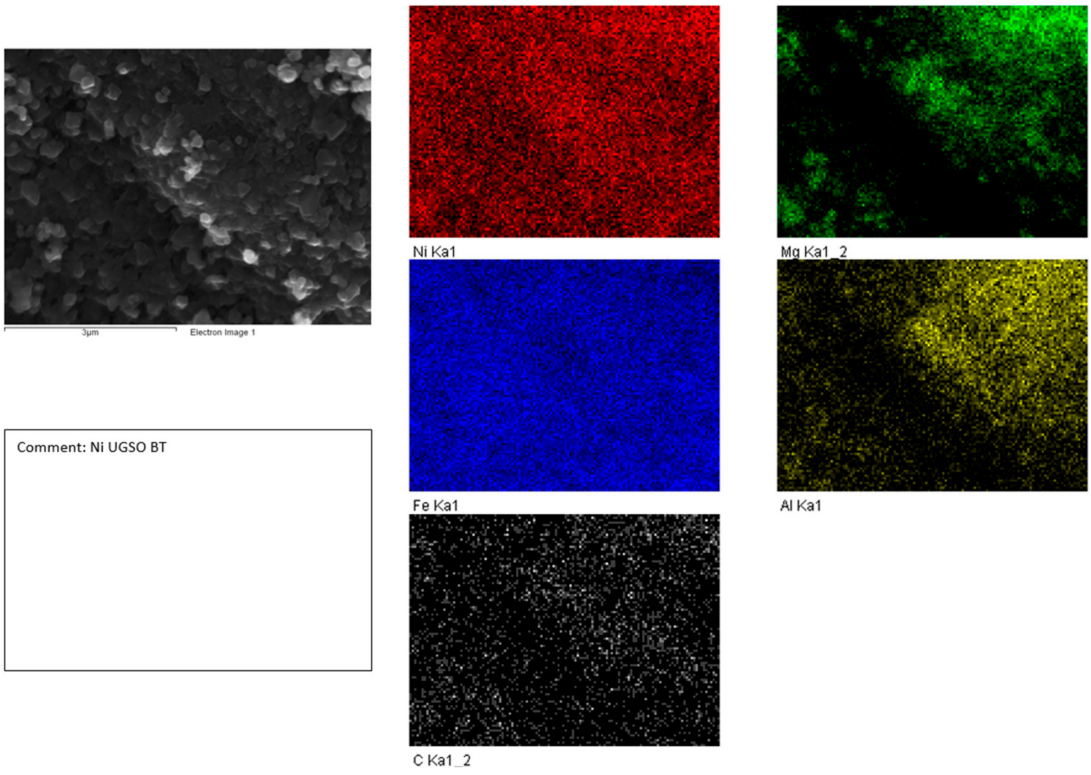

Figure 9. Mapping analysis of Ni-UGSO BT.

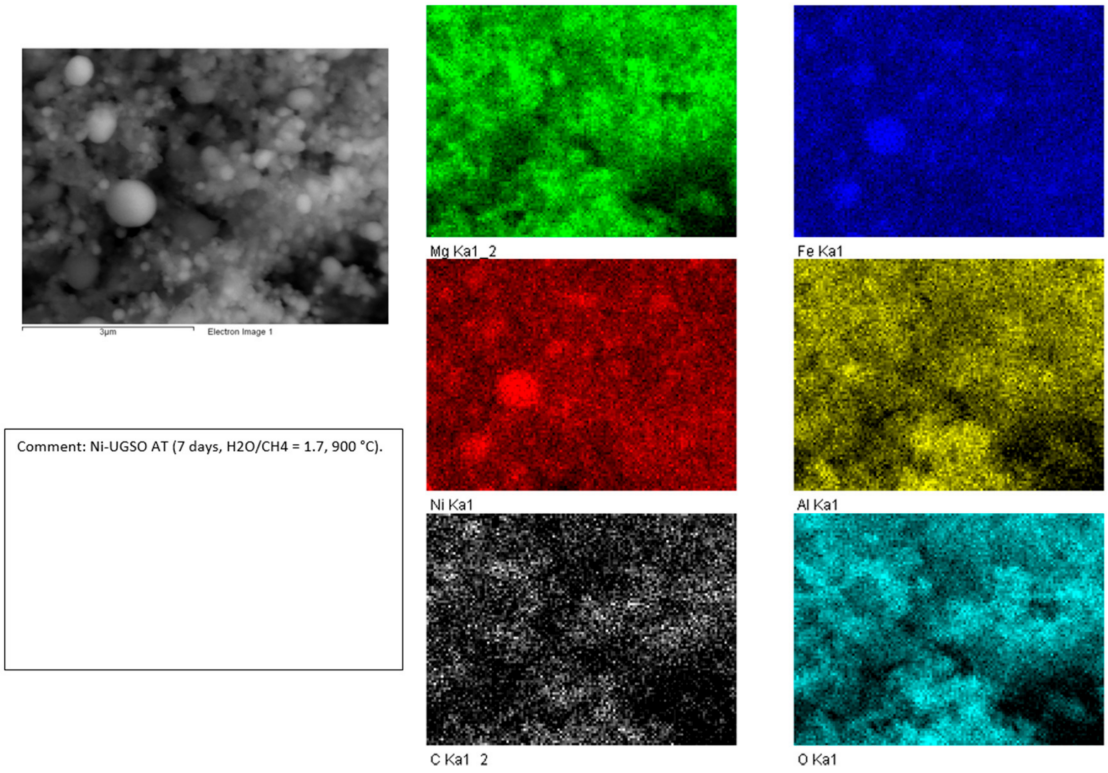

Figure 10. Mapping analysis of Ni-UGSO AT (7 days, H_2O/CH_4 = 1.7, 900 °C).

2.5. Ni-UGSO Performance as a Catalyst for Mixed Methane Dry and Steam Reforming

For this study, Ni-UGSO stability was validated in DRM using a Q_{CO2} = 7.29 mL/min, Q_{CH4} = 7.55 mL/min and Q_{H2O} = 1.04 mL/min) without Ar (H_2O/CH_4 = 0.14, $CO_2/_{CH4}$ = 0.97 and $CH_4/(CO_2 + H_2O)$ = 0.91) for 74 h. Three reaction temperature levels (828 °C, 847 °C and 896 °C) were used over these 74 h TOS.

CH_4 conversion remained stable at each temperature level: 80% at 828 °C (26 h), 85% at 847 °C (24 h) and 95% at 896 °C (24 h) (Figure 11).

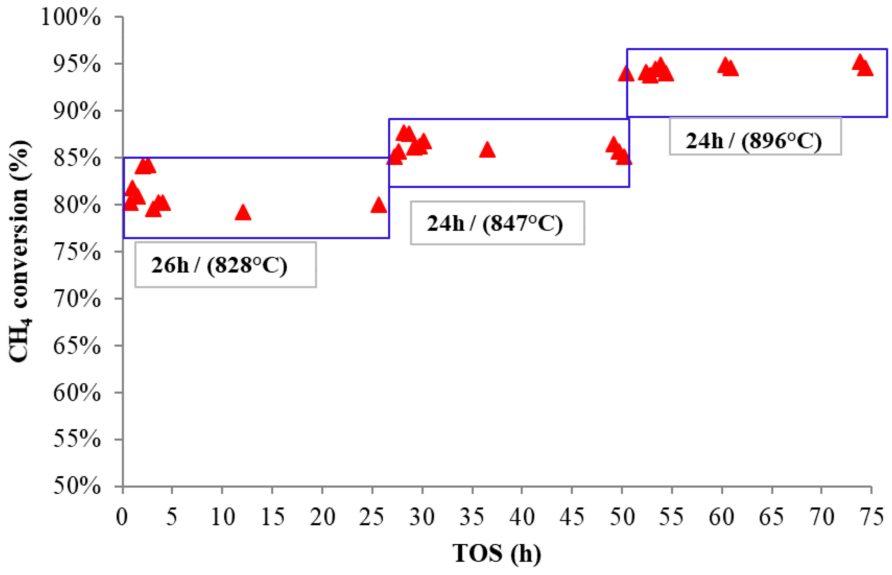

Figure 11. Catalytic performances of Ni-UGSO on mixed methane dry and steam reforming (CO_2/CH_4 = 0.97 and H_2O/CH_4 = 0.15).

Referring to Figure S16 (Supplementary Materials), XRD of the Ni-UGSO catalyst used during 74 h of reaction showed that it had the same structure as that used for 4 h under the same conditions without any carbon deposition as illustrated by the SEM-EDX analyses (Figure S17, Supplementary Materials).

The results were the same order of magnitude as those obtained by Nakhaei et al. [34] in the mixed CO_2 and steam reforming of methane. Experimental conditions were close to ours except for the temperature, which was slightly lower, and the GHSV, which was higher: 750 °C, $CH_4/(CO_2 + H_2O) = 0.87$, $CH_4/CO_2 = 1$ and $CO_2/H_2O = 6.4$ and a GHSV = 20 L/(h·g). Different Ni/MgO/α-Al_2O_3 catalysts were prepared with Mg 1 wt% and Ni 1 to 5 wt%. Unlike our catalyst, which was used as it was produced, the Nakhaei et al. [34] catalyst underwent a pre-reduction. Results showed an increase of CH_4 conversion from 54% to 74% upon increasing Ni loading from 1% to 5%. The authors indicated that such performance is attributed to solid solution NiO–MgO and that the reactions reach conversions and yields close to thermodynamic equilibrium.

By studying a mixed DRM and SRM, at a ratio ($CO_2 + H_2O/CH_4$) closer to 1, at atmospheric pressure and at temperature greater than or equal to 800 °C, Jabbour et al. [35] recently discovered that the use of MgO (or CaO) basic promoters in Ni 5% Mg 5% Al_2O_3 or Ni 5% Ca 5% Al_2O_3 catalysts provided remarkable activity, stability and selectivity in syngas. Compared to unpromoted Ni 5% and Ni 10% Al_2O_3, after 40 h of reaction, a significant reduction in deposited carbon was observed with improvement in the reactivity and purity of the synthesis gases obtained.

Similarly, Koo et al. [24] and Mehr et al. [36] led mixed steam and dry reforming of methane without and in the presence of MgO-assisted, Ni-impregnated on Al_2O_3 catalysts. The authors deduced that the addition of MgO had a positive effect on the eliminating carbon deposition and on reactivity and selectivity.

3. Discussion

The new Ni-UGSO catalyst, resulting from upgrading of a mining residue with a negative UGSO value, has demonstrated catalytic performance at least equal to that of the various homologous nickel-based catalysts described in the literature. Besides the catalytic performance in DRM, SRM and MRM occurring near thermodynamic equilibrium, no carbon deposit was detected, especially as it demonstrated good resistance to sulfides (low quantity).

All of these promising results are attributed to the different constituent elements of the UGSO mining residue despite not being catalytically active by themselves (Fe, Mg, Al, Ca, Mn, V, Ti, Cr, Na, Si, K, P, Zr and Zn oxides and spinels). Indeed, the addition of Ni allows different interactions to be triggered synergistically between the components of UGSO and the active metal (Ni). It should be remembered that most of these elements, used as supports or promoters, have been the subject of several recommendations from studies aimed at reducing or eliminating the formation of coke on Ni-based catalysts. As demonstrated in our previous work [28], the reducing medium during the DRM causes a reduction of $NiFe_2O_4$ spinel compound into FeO, NiO and metallic Ni, Fe and some other alloys such as FeNi, $FeNi_3$ and Fe_3Ni_2. As described by Benrabaa et al. [37,38], the fact that Ni is well dispersed in this alloy minimizes the formation of carbon deposit as much as possible.

Regarding the other elements constituting the residue used as a promoter, our interest has focused on magnesium oxide (MgO) without neglecting the role of other elements whose effect is described in several articles in the literature.

In fact, several studies have demonstrated the positive effects of MgO as promoters with significant Lewis basicity and as an oxide easily forming a solid solution with Ni oxide (MgO–NiO). On the one hand, the presence of basic Lewis sites (O^{2-}) [39] will reinforce the chemisorption of CO_2 on these sites, and the adsorbed CO_2 reacts with carbon. This reaction shifts the equilibrium of the reaction from Boudouard to CO ($CO_2 + C \rightarrow 2CO$), promoting the coke elimination reaction, which considerably reduces the deposition of

surface carbon [40]. On the other hand, Son et al. [41] reported that, with its oxygen storage capacity, MgO could remove carbon formed on the surface of a catalyst by its oxidation with liberated oxygen. The high nickel activity and carbon resistance are also attributed to the formation of a solid solution of NiO in MgO.

Wang et al. [42] explain that the solid NiO–MgO solution could have two main phases: A solid NiO–MgO solution with a high Ni content in the outer layer and a solid NiO–MgO solution with a very low Ni content in the mass. Thus, Ni particles can diffuse from the outer layer to the deeper layer to form a more stable structure at high temperatures, which prevents the sintering of nickel particles for high-temperature reactions. In addition, Hu and Ruckenstein [39] indicate that, due to the strong interaction between NiO and MgO, the coalescence or aggregation of Ni, which stimulates carbon formation, is inhibited. This strong interaction between NiO and MgO could also weaken the donor character of Ni, thereby preventing disproportionation of CO. Bradford et al. [43] have shown that the Ni/MgO catalyst is both active and stable during 44 h of dry reforming of CH_4. Such performance and resistance to coke deposition were explained by the formation of a solid solution of MgO–NiO due to the strong dissolution of NiO in MgO. This partially reducible solution is reported to stabilize metal Ni and enhance resistance to carbon deposition. Likewise, the good catalytic performance of the Ni/$MgAl_2O_4$ spinel, obtained by the addition of MgO to the Ni/Al_2O_3 system, is attributed to a greater CO_2 adsorption capacity due to the increase in the density of the basic Lewis sites of on the surface of the catalyst [25,44].

4. Materials and Methods

4.1. Materials

4.1.1. Constitutive Elements of the UGSO Residue

Table 3 shows the constitutive elements of the UGSO residue obtained by ICP-MS analysis. Fe, Mg and Al are the main elements.

4.1.2. Particle Size Distribution

The first raw UGSO (UGSO-L1) received from our industrial partner was milled in a mortar and sieved to collect the fraction corresponding to sizes below 53 µm (smaller sieve); this fraction was chosen for the preparation of the catalytic formulations Table 4 shows the particle size distribution of this fraction of UGSO.

Table 4. Particle size distribution of UGSO-L1.

	d (0.1)	d (0.2)	d (0.5)	d (0.8)	d (0.9)
UGSO (µm)	1.75	6.51	25.85	48.07	61.42

4.2. Ni-UGSO Preparation via Improved Solid-State Reaction

Ni-UGSO was prepared following the improved solid-state reaction developed in a previous work [26–28]. To study the effect of the content of Ni, 3, 6, 9, 10 and 13 wt% were added. Table 5 shows particle size distribution and Ni-UGSO (13 wt%) compared to UGSO.

Table 5. Particle size distribution of Ni-UGSO (13 wt%).

	d (0.1)	d (0.2)	d (0.5)	d (0.8)	d (0.9)
Ni-UGSO (µm)	1.24	3.71	20.34	46.83	56.97

4.3. Catalysts Characterization

Our previous work [26] describes various characterization techniques used to analyze the new Ni-UGSO catalyst, such as X-ray diffraction (XRD), scanning electron microscopy-energy dispersive X-ray (SEM-EDX), temperature-programmed reduction (TPR), X-ray

photoemission spectrometry (XPS), thermogravimetric analysis (TGA) coupled with mass spectroscopy (MS) and BET specific surface.

4.4. Use of Ni-UGSO as a Catalyst

The produced Ni-UGSO was used as a catalyst for DRM, SRM and mixed methane reforming (MRM).

The experiments were conducted under the same conditions as those described in a previous work [27] at atmospheric pressure in a differential fixed-bed catalytic reactor (Figure 12) using 0.3–0.5 g of Ni-UGSO. Total flow rate and space velocity were 15 mL/min and 3000 mL/(h·gcat) respectively.

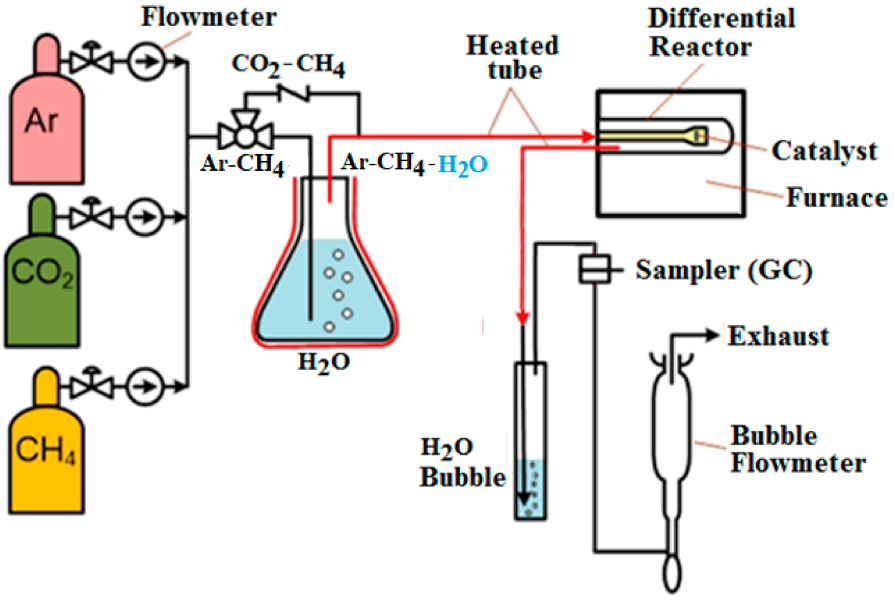

Figure 12. Schematic of DRM, SMR and mixed reforming microreactor.

Gases were fed from commercial gas cylinders (supplied by Praxair, Sherbrooke, Québec, Canada): CH_4 (99%), CO_2 (99%) and Ar (99%). Flow rates of CO_2 and CH_4 were adjusted by the AALBORG-type mass flow controller (Model GFC17) (supplied by AALBORG, Orangeburg, NY, USA). Flow rates of the reactants and the reaction products were also measured by a bubble meter. In the case of SRM, a mixture of argon and methane is saturated in the bubbler, and the desired amount of water is regulated using the water temperature control. At saturation at 73 °C, the partial pressure of water vapour is 354.45 hPa. For 32% of CH_4 in Ar, the CH_4 partial pressure is 212.97 hPa corresponding to a H_2O/CH_4 ratio = 1.7. The effluents were analyzed using a gas chromatograph (Varian CP-3800) (supplied by Varian, Inc, Walnut Creek, CA, USA) equipped with Hayesep and Molsieve columns and with thermal conductivity (TCD) and flame ionization (FID) detectors. Helium and nitrogen were used as carrier gases, and hydrogen and air were used for the detector flame. The flow rates of gases are: 18.8 mL/min (He), 21.2 mL/min (N_2), 30 mL/min (H_2) and 300 mL/min (air). The columns and the detector were heated to 175 °C at a rate of 20 °C/min. H_2, CO, CH_4, and CO_2 are the main gases detected. Calibration was performed using gas mixture standards at different concentrations. The concentrations of reactants were added to the experimental conditions of each type of test.

4.5. Reaction Metrics

Conversion of CH_4 was calculated by Equation (1). H_2 and CO yields as defined by Equations (2) and (3) respectively:

$$X_i(\%) = \frac{F_{i,\,in} - F_{i,\,out}}{F_{i,\,in}} \times 100 \quad (1)$$

$$Y_{H_2}(\%) = \frac{F_{H_2}}{2 \times F_{CH_{4,\,in}}} \times 100 \quad (2)$$

$$Y_{CO}(\%) = \frac{F_{CO}}{F_{CH_{4,\,in}} + F_{CO_{2,\,in}}} \times 100 \quad (3)$$

where $F_{i,in}$ or $F_{i,out}$ is the flow rate of each component in the feed or effluent.

Concerning the experimental errors of the various reforming results, we proceeded, for brevity and figure-readability reasons, to the calculation of the standard deviations of the material balances (atomic: C, H, O) instead of error bars: C (1.4%), O (3.9%) and H (6.3%).

As shown in Table 6, the standard deviation was calculated from the average of the averages of each study below (Table 7):

- influence of the active phase content on the catalytic activity;
- influence of catalyst calcination time;
- representativeness of UGSO mining residue lots;
- Ni-UGSO sulfur poisoning resistance;
- Ni-UGSO performance as a catalyst for steam methane reforming (SRM);
- Ni-UGSO performance as a catalyst for mixed methane dry and steam reforming (MRM).

Table 6. Error mean and standard deviation.

	C	O	H
Error mean	2.59%	4.47%	3.99%
Standard deviation	1.35%	3.93%	6.28%

The following table shows the error mean and standard deviation.

Table 7. Average errors on atomic carbon, hydrogen and oxygen for of each study.

	C	O	H
Effect of Ni content	3.58%	8.03%	8.81%
Effect of calcination time	2.55%	3.54%	7.87%
Ni-UGSO sulfur poisoning resistance	2.54%	4.93%	−7.84%
Representativeness of UGSO mining residue lots	−0.18%	−1.35%	9.31%
Steam methane reforming (SMR)	4.07%	10.37%	6.63%
Mixed methane dry and steam reforming	2.97%	1.31%	−0.84%

This means that our confidence interval for carbon was 2.59 ± 1.35.

5. Conclusions

In this work, UGSO mining waste was doped with Ni using a recently published improved solid-state reaction protocol; the resulting spinelized structure proved to be a robust and highly active Ni-UGSO reforming catalyst. DRM, SRM, MRM and sulfur poisoning resistance were chosen to test the catalytic performance and robustness of this new catalyst. The DRM and SRM reactions demonstrated an excellent hydrocarbon conversion and hydrogen yield and the H_2/CO ratios obtained in the product were close to 1 (for

DRM) and close to 3 (for SRM); these ratios are nearly those expected for thermodynamic equilibrium in the experimental conditions tested.

As mentioned before, the constituent elements of the UGSO had a positive effect on the performance of the catalyst, allowing a good dispersion and interaction of Ni in the UGSO. As in previously published works in this area, our results also show that, in addition to the effect of certain Ni_xFe_y alloys, the Ni inside the spinel structure leads to a high stability and a high dispersion of the particles of the active metal, limiting the growth of the Ni particles preventing the formation of carbon while maintaining a high catalytic activity. Likewise, the basic character of components like MgO acts as catalyst promoters by inhibiting the carbon formation on the catalyst surface and stimulating the solid carbon gasification. Furthermore, the protection of the metallic Ni (which is formed during reduction) by the solid solution Ni/NiO/MgO could explain the activity and the stability of the catalyst.

In conclusion, of these four types of investigation in this work, CH_4 conversion in SRM remained stable at around 98% during the 168 h TOS of reaction under 1 bar at 900 °C at a molar H_2O/CH_4 = 1.7. Likewise, in DRM, CH_4 conversion rapidly reaches 92% and remains stable over 168 h TOS under 1 bar at 810 °C and at molar CO_2/CH_4 = 1.2. For mixed CH_4 reforming using a molar ratio of H_2O/CH_4 = 0.15 and CO_2/CH_4 = 0.97 for 74 h under 1 bar and three reaction temperature levels (828 °C, 847 °C and 896 °C), CH_4 conversion remains stable at each temperature level: 80% at 828 °C (26 h), 85% at 847 °C (24 h) and 95% at 896 °C (24 h). Five levels of Ni mass contents (3%, 6%, 9%, 10% and 13%) in the Ni-UGSO formulation have been compared at 840 °C and a molar CO_2/CH_4 of 1.25. The best performances was observed with the 10% *w*/*w* Ni catalyst. Statistically similar performance was obtained with the 13% *w*/*w* Ni catalyst. The catalysts Ni-UGSO calcined at 900 °C for 3 h and 12 h give the same catalytic performances at 840 °C with a CO_2/CH_4 = 1.2. Even though the composition of the two batches of UGSO used to produce the Ni-UGSO catalytic formulation are slightly different, both Ni-UGSO catalysts demonstrated equivalent performance during DRM at 840 °C and molar CO_2/CH_4 = 1.2. The catalyst showed no deactivation up to 5.5 ppm of H_2S. A slight deactivation (3%) was observed at 12 ppm and remained stable throughout the 1 h exposure of the catalyst to H_2S.

Supplementary Materials: The following are available online at https://www.mdpi.com/article/10.3390/catal11070771/s1. Figure S1: Evolution of free enthalpies (ΔG (T)) of DRM and SRM reactions as a function of temperature, Figure S2: CH_4 and CO_2 conversions and composition of gas mixtures and graphitic carbon at thermodynamic equilibrium for the DRM reaction, Figure S3: Thermodynamic equilibrium H_2/CO ratio for the DRM reaction, Figure S4: CH_4 and CO_2 conversions and composition of gas mixtures and graphitic carbon at thermodynamic equilibrium for the SRM reaction, Figure S5: Thermodynamic equilibrium H_2/CO ratio for the SRM reaction, Figure S6: Effect of Ni content: evolution of CO_2 conversion as a function of time at 842 °C, CO_2/CH_4 = 1.25, Figure S7: Effect of Ni content: evolution of H_2 yield as a function of time at 842 °C, CO_2/CH_4 = 1.25, Figure S8: Effect of Ni content: evolution of H_2/CO ratio as a function of time at 842 °C, CO_2/CH_4 = 1.25, Figure S9: Mapping study as function of Ni-loading, Figure S10: XRD catalysts calcined at 900 °C for 1 h, 3 h and 12 h, Figure S11: XRD of the two lots of UGSO compared to that of the UGSO L1 calcined at 900 °C/12 h, Figure S12: XRD of the of UGSO-L2 compared to that of the UGSO-L3 calcined at 900 °C/12 h, Figure S13: XRD of Ni-UGSO catalysts from 2 lots calcined at 900 °C for 1 h, Figure S14: XRD of spent Ni-UGSO catalysts without and with H_2S, Figure S15: XRD of Ni-UGSO used for 7 days at the SRM (H_2O/CH_4 = 1.7, 900 °C) compared to the fresh catalyst Ni-UGSO BT, Figure S16: XRD of used catalyst Ni-UGSO AT (4 h & 74 h) (CO_2/CH_4 = 0.97 and H_2O/CH_4 = 0.15), Figure S17: SEM-EDX of used catalyst Ni-UGSO AT (4 h & 74 h) (CO_2/CH_4 = 0.97 and H_2O/CH_4 = 0.15).

Author Contributions: M.C., co-inventor with N.A. of the catalytic formulations tested has contributed in choosing the catalytic formulations, the experimental protocols, technically in adopting the most appropriate experimental protocols and in the scientific interpretation of the results. N.A., the corresponding author, is the scientific and technical director of the R&D program. He has con-

tributed to choosing the experimental protocols and the catalytic formulations. He has also worked with the first author in reviewing the first draft and finalizing the manuscript. All authors have read and agreed to the published version of the manuscript.

Funding: This research was funded by FRQNT (Fonds de recherche du Quebec_Nature and technologies), grant number: 2017-MI-202929.

Data Availability Statement: We would like to share these data; however, there are confidentiality issues; these data are used for the advancement of our current work in collaboration with our industrial partners.

Acknowledgments: We would like to thank FRQNT (Fonds de recherche du Quebec_Nature and technologies) for the financial support of this project. Special thanks to Guillaume Hudon and Yves Pepin of Rio Tinto Iron and Titanium (RTIT), for both funding and for providing the metallurgical residue and their technical support. We thank also Sonia Blais, Stephane Gutierrez, Carl Saint-Louis and Charles Bertrand of PRAM (Plateforme de recherche et d'analyse des matériaux) at Université de Sherbrooke for their technical assistance in instrumental analyses.

Conflicts of Interest: The authors declare no conflict of interest.

References

1. Rostrup-Nielsen, J.R.; Sehested, J.; Nørskov, J.K. Hydrogen and synthesis gas by steam- and CO_2 reforming. *Adv. Catal.* **2002**, *47*, 65–139. [CrossRef]
2. Levent, M.; Gunn, D.J.; Ali El-Bousiffi, M. Production of hydrogen-rich gases from steam reforming of methane in an automatic catalytic microreactor. *Int. J. Hydrogen Energy* **2003**, *28*, 945–959. [CrossRef]
3. Iulianelli, A.; Manzolini, G.; De Falco, M.; Campanari, S.; Longo, T.; Liguori, S.; Basile, A. H_2 production by low pressure methane steam reforming in a Pd–Ag membrane reactor over a Ni-based catalyst: Experimental and modeling. *Int. J. Hydrogen Energy* **2010**, *35*, 11514–11524. [CrossRef]
4. Tullo, A.H. Dry reforming puts CO_2 to works. *Chemical & Engineering News*, 25 April 2016, p. 17. Available online: https://cen.acs.org/articles/94/i17/Dry-reforming-puts-CO2-work.html?ref=search_results (accessed on 24 June 2021).
5. Xu, L.; Song, H.; Chou, L. Carbon dioxide reforming of methane over ordered mesoporous NiO-MgO-Al_2O_3 composite oxides. *Appl. Catal. B Environ.* **2011**, *108*, 177–190. [CrossRef]
6. Seo, H.O.; Sim, J.K.; Kim, K.D.; Kim, Y.D.; Lim, D.C.; Kim, S.H. Carbon dioxide reforming of methane to synthesis gas over a TiO_2-Ni inverse catalyst. *Appl. Catal. A Gen.* **2013**, *451*, 43–49. [CrossRef]
7. Ondrey, G. Making Co-Rich Syngas While Avoiding Carbon Formation. Available online: https://www.chemengonline.com (accessed on 13 November 2019).
8. Mark, M.F.; Mark, F.; Maier, W.F. Reactions kinetics of the CO_2 reforming of methane. *Chem. Eng. Technol.* **1997**, *20*, 361–370. [CrossRef]
9. Tsang, S.C.; Claridge, J.B.; Green, M.L. Recent advances in the conversion of methane to synthesis gas. *Catal. Today* **1995**, *23*, 3–15. [CrossRef]
10. Corthals, S.; Van Nederkassel, J.; Geboers, J.; De Winne, H.; Van Noyen, J.; Moens, B.; Sels, B.; Jacobs, P. Influence of composition of $MgAl_2O_4$ supported $NiCeO_2ZrO_2$ catalysts on coke formation and catalyst stability for dry reforming of methane. *Catal. Today* **2008**, *138*, 28–32. [CrossRef]
11. Menegazzo, F.; Signoretto, M.; Pinna, F.; Cauton, P.; Pernicone, N. Optimization of bimetallic dry reforming catalysts by temperature programmed reaction. *Appl. Catal. A Gen.* **2012**, *439–440*, 80–87. [CrossRef]
12. De Liobet, S.; Pinilla, J.L.; Moliner, R.; Suelves, I. Relationship between carbon morphology and catalyst deactivation in the catalytic decomposition of biogas using Ni, Co and Fe based catalysts. *Fuel* **2015**, *139*, 71–78. [CrossRef]
13. Nagaoka, K.; Seshan, K.; Lercher, J.A.; Aika, K. Activation mechanism of methane derived coke (CH_x) by CO_2 during dry reforming of methane comparison for Pt/Al_2O_3 and Pt/ZrO_2. *Catal. Lett.* **2000**, *70*, 109–116. [CrossRef]
14. Provendier, H.; Petit, C.; Estournès, C.; Libs, S.; Kiennemann, A. Stabilisation of active nickel catalysts in partial oxidation of methane to synthesis gas by iron addition. *Appl. Catal. A Gen.* **1999**, *180*, 163–173. [CrossRef]
15. Salhi, N.; Boulahouache, A.; Petit, C.; Kiennemann, A.; Rabia, C. Steam reforming of methane to syngas over $NiAl_2O_4$ spinel catalysts. *Int. J. Hydrogen Energy* **2011**, *36*, 11433–11439. [CrossRef]
16. Abatzoglou, N.; Fauteux-Lefebvre, C.; Blanchard, J.; Gitzhofer, F. Steam Reforming of Hydrocarbons over a Ni-Alumina Spinel Catalyst. *J. Power Sources* **2010**, *195*, 3275–3283.
17. Fauteux-Lefebvre, C.; Abatzoglou, N.; Braidy, N.; Achouri, I.E. Diesel steam reforming with a nickel–alumina spinel catalyst for solid oxide fuel cell application. *J. Power Sources* **2011**, *196*, 7673–7680. [CrossRef]
18. Achouri, I.E.; Abatzoglou, N.; Fauteux-Lefebvre, C.; Braidy, N. Diesel steam reforming: Comparison of two nickel aluminate catalysts prepared by wet-impregnation and co-precipitation. *Catal. Today* **2013**, *207*, 13–20. [CrossRef]
19. Wang, S.; Lu, G.Q. Effects of promoters on catalytic activity and carbon deposition of Ni/γ-Al_2O_3 catalysts in CO_2 reforming of CH_4. *J. Chem. Technol. Biot.* **2000**, *75*, 589–595. [CrossRef]

20. Sutthiumporn, K.; Kawi, S. Promotional effect of alkaline earth over Ni-La_2O_3 catalyst for CO_2 reforming of CH_4: Role of surface oxygen species on H_2 production and carbon suppression. *Int. J. Hydrogen Energy* **2011**, *36*, 14435–14446. [CrossRef]
21. Al-Fatesh, A.S.; Fakeeha, A.H.; Abasaeed, A.E. Effects of selected promoters on Ni/γ-Al_2O_3 Catalyst performance in methane dry reforming. *Chin. J. Catal.* **2011**, *32*, 1604–1609. [CrossRef]
22. Luna, A.E.; Iriarte, M.E. Carbon dioxide reforming of methane over a metal modified Ni-Al_2O_3 catalyst. *Appl. Catal. A Gen.* **2008**, *343*, 10–15. [CrossRef]
23. Siahvashi, A.; Adesina, A.A. Synthesis gas production via propane dry (CO_2) reforming: Influence of potassium promotion on bimetallic Mo-Ni/Al_2O_3. *Catal. Today* **2013**, *214*, 30–41. [CrossRef]
24. Koo, K.Y.; Roh, H.S.; Seo, Y.T.; Seo, D.J.; Yoon, W.L.; Park, S.B. Coke study on MgO-promoted Ni/Al_2O_3 catalyst in combined H_2O and CO_2 reforming of methane for gas to liquid (GTL) process. *Appl. Catal. A Gen.* **2008**, *340*, 183–190. [CrossRef]
25. Ranjbar, A.; Rezaei, M. Preparation of nickel catalysts supported on CaO.2Al_2O_3 for methane reforming with carbon dioxide. *Int. J. Hydrogen Energy* **2012**, *37*, 6356–6362. [CrossRef]
26. Chamoumi, M.; Abatzoglou, N.; Blanchard, J.; Iliuta, M.C.; Larachi, F. Dry reforming of methane with a new catalyst derived from a negative value mining residue spinellized with nickel. *Catal. Today* **2017**, *291*, 86–98. [CrossRef]
27. Abatzoglou, N.; Chamoumi, M. Process for Producing Catalysts from Metallurgical Tailings and Catalysts Produced Therefrom. U.S. Patent WO/2017/011906A1, 26 January 2017.
28. Chamoumi, M.; Abatzoglou, N. $NiFe_2O_4$ production from α-Fe_2O_3 via an improved solid state reaction and its use as a dry reforming catalyst. *Can. J. Chem. Eng.* **2016**, *94*, 1801–1808. [CrossRef]
29. Requies, J.; Cabrero, M.A.; Barrio, V.L.; Guemez, M.B.; Cambra, J.F.; Arias, P.L.; Perez-Alonso, F.J.; Ojeda, M.; Pena, M.A.; Fierro, J.L.G. Partial oxidation of methane to syngas over Ni/MgO and Ni/La_2O_3 catalysts. *Appl. Catal. A Gen.* **2005**, *289*, 214–223. [CrossRef]
30. Chamoumi, M. Nouvelle Génération de Catalyseurs Supportés par Valorisation d'un Résidu d'Enrichissement (Procédé UGS) d'une Scorie de TiO_2: Le Catalyseur Ni-UGSO Appliqué au Reformage de Méthane [New Generation of Catalysts Supported by Upgrading an Enrichment Residue (UGS Process) of TiO_2 Slag: Ni-UGSO Catalyst Applied to Methane Reforming]. Ph.D. Thesis, Université de Sherbrooke, Sherbrooke, QC, Canada, 2017.
31. Blondel Dega, F.; Abatzoglou, N. H_2S poisoning and pegeneration of a nickel spinellized catalyst prepared from waste metallurgical residues, during dry autothermal methane reforming. *Catal. Lett.* **2019**, *149*, 1730–1742. [CrossRef]
32. Rostrup-Nielsen, J.R. Catalytic steam reforming. In *Catalysis: Science and Technology*; Anderson, J.R., Boudart, M., Eds.; Springer-Verlag: Berlin/Heidelberg, Germany; New York, NY, USA; Tokyo, Japan, 1984; pp. 1–117.
33. Bimbela, F.; Chen, D.; Ruiz, J.; Garcia, L.; Arauzo, J. Ni/Al coprecipitated catalysts modified with magnesium and copper for the catalytic steam reforming of model compounds from biomass pyrolysis liquids. *Appl. Catal. B Environ.* **2012**, *119–120*, 1–12. [CrossRef]
34. Nakhaei Pour, A.; Mousavi, M. Combined reforming of methane by carbon dioxide and water: Particle size effect of Ni-Mg nanoparticles. *Int. J. Hydrogen Energy* **2015**, *40*, 12985–12992. [CrossRef]
35. Jabbour, K.; Massiani, P.; Davidson, A.; Casale, S.; El Hassan, N. Ordered mesoporous "one-pot" synthesized Ni-Mg (Ca)-Al_2O_3 as effective and remarkably stable catalysts for combined steam and dry reforming of methane (CSDRM). *Appl. Catal. B Environ.* **2017**, *201*, 527–542. [CrossRef]
36. Mehr, Y.; Jozani, K.J.; Pour, A.N.; Zamani, Y. Influence of MgO in the CO_2—Steam reforming of methane to syngas by NiO/MgO/α-Al_2O_3 catalyst. *React. Kinet. Catal. Lett.* **2002**, *75*, 267–273. [CrossRef]
37. Benrabaa, R.; Boukhlouf, H.; Lofberg, A.; Rubbens, A.; Vannier, R.N.; Bordes-Richard, E.; Barama, A. Nickel ferrite spinel as catalyst precursor in the dry reforming of methane: Synthesis, characterization and catalytic properties. *J. Nat. Gas. Chem.* **2012**, *21*, 595–604. [CrossRef]
38. Benrabaa, R.; Lofberg, A.; Rubbens, A.; Bordes-Richard, E.; Vannier, R.N.; Barama, A. Structure, reactivity and catalytic properties of nanoparticles of nickel ferrite in the dry reforming of methane. *Catal. Today* **2013**, *203*, 188–195. [CrossRef]
39. Hu, Y.H.; Ruckenstein, E. Characterization of a highly effective NiO/MgO solid solution catalyst in CO_2 reforming of CH_4. *Catal. Lett.* **1997**, *43*, 71–77. [CrossRef]
40. Xu, L.; Song, H.; Chou, L. Ordered mesoporous MgO-Al_2O_3 composite oxides supported Ni based catalysts for CO_2 reforming of CH_4: Effects of basic modifier and mesopore structure. *Int. J. Hydrogen Energy* **2013**, *38*, 7307–7325. [CrossRef]
41. Son, I.H.; Lee, S.J.; Roh, H.S. Hydrogen production from carbon dioxide reforming of methane over highly active and stable MgO promoted Co-Ni/α-Al_2O_3 catalyst. *Int. J. Hydrogen Energy* **2014**, *39*, 3762–3770. [CrossRef]
42. Wang, T.; Chang, J.; Cui, X.; Zhang, Q.; Fu, Y. Reforming of raw fuel gas from biomass gasification to syngas over highly stable nickel–magnesium solid solution catalysts. *Fuel Process. Technol.* **2006**, *87*, 421–428. [CrossRef]
43. Bradford, M.; Vannice, M. CO_2 reforming of CH_4. *Catal. Rev.* **1991**, *41*, 1–42. [CrossRef]
44. Fakeeha, A.H.; Naeem, M.A.; Khan, W.U.; Abasaeed, A.E.; Al-Fatesh, A.S. Reforming of methane by CO_2 over bimetallic Ni-Mn/γ-Al_2O_3 catalyst. *Chin. J. Chem. Phys.* **2014**, *27*, 214–220. [CrossRef]